THE ASTROPHYSICAL JOURNAL, 397:664–673, 1992 October 1

THE *HUBBLE SPACE TELESCOPE* OBSERVATIONS OF X-RAY NOVA MUSCAE 1991 AND ITS SPECTRAL EVOLUTION[1]

F. H. CHENG,[2,3] KEITH HORNE,[2] N. PANAGIA,[2,4,5] C. R. SHRADER,[6] R. GILMOZZI,[2,4,7]
F. PARESCE,[2,4,8] AND N. LUND[9]

Received 1992 January 7; accepted 1992 April 6

ABSTRACT

We report *HST*/Faint Object Spectrograph (FOS) and Faint Object Camera (FOC) observations of X-ray Nova Muscae 1991 obtained on 1991 May 14–15. The FOS spectrum covering 1581–4807 Å shows a clear 2200 Å absorption feature. With a fit to the continuum considering the interstellar extinction and a power-law spectrum ($f_\nu \propto \nu^\alpha$), we determine a color excess $E(B-V) \sim 0.29$ and a power-law slope of $\alpha \sim 0.30$, which approximates a canonical accretion disk spectrum. By fitting a simple model of a steady state blackbody accretion disk around a black hole to the FOS spectrum and multiepoch data in the optical, UV, and X-ray bands, we estimate the lower limit mass of the central compact object $M_{\rm min}$, the radius of the accretion disk $R_{\rm out}$, the maximum orbital period $P_{\rm max}$, and the upper limit mass transfer rate $\dot{M}_{\rm max}$ during the decline for several assumed values of the disk inclination angle i and distance D to the source. We find that $\dot{M}$ decays exponentially with a characteristic time of $\sim$43 days. The cooling front predicted by the disk instability models to occur in the outer disk when $T < 10^4$ K should have been observable, but was not seen.

Subject headings: novae, cataclysmic variables — stars: individual (Nova Muscae 1991) — ultraviolet stars

1. INTRODUCTION

X-ray novae are believed to be binary systems in which the primary star is a neutron star or a black hole. The best-studied member of this small class (including Nova Muscae 1991) is V616 Mon = A0620−00, for which McClintock & Remillard (1986) and Haswell & Shafter (1990) have estimated its strict lower limits of 3.2 and 3.8 $M_\odot$, respectively, for the central compact object, suggesting that it is a black hole. More recently Casares, Charles, & Naylor (1992) have found that V404 Cyg has a mass function of 6.3 $M_\odot$, the largest yet in a low-mass X-ray binary (LMXB).

Unlike classical novae, which are understood to be thermonuclear explosions on the surfaces of accreting white dwarfs, the X-ray novae are considered by some to be accretion events. The disk instability model has had some success in explaining dwarf novae as accretion events onto white dwarfs in cataclysmic variables (Osaki 1974). When applied to novae containing massive compact objects, the disk instability model has some difficulty in accounting for the observed recurrence times, that is, 60 yr for V616 Mon, and 51 yr for V404 Cyg (Mineshige & Wheeler 1989), unless an extremely low value of the viscosity parameter or a low mass transfer rate is adopted. Detailed observation and modeling of the spectral development of X-ray novae on the decline from outburst provides an opportunity to test this disk instability model further.

Nova Muscae 1991 was discovered in early 1991 January, as a transient X-ray source (GRS 1121−68 = GS 1124−683) reported by the WATCH/Granat Team (Lund & Brandt 1991) and the Ginga Team (Makino 1991). Nova Muscae offers us a good opportunity to study in detail the properties and the evolution of an object that may test the disk instability model and the black hole hypothesis.

The X-ray spectra of Nova Muscae obtained by Granat on 1991 January 16–17 and 17–18 can be described as a power law with photon index $\sim$2.2–2.3. The one observed on 1991 January 20–21 extended from 3.5 to 600 eV with no exponential cutoff (Sunyaev, Jourdian, & Laurent 1991a). The optical counterpart of Nova Muscae 1991 was identified at ESO (Della Valle & Jarvis 1991; Della Valle, Jarvis, & Wist 1991a, 1991b) with a bluish star with $V \sim 14$ mag on 1991 January 13. It promptly brightened to $\sim$13.4 mag on 1991 January 15, and then declined at an approximate rate of 0.15 mag week^{-1}. Photometric and spectroscopic observations were carried out at ESO with the New Technology Telescope (NTT), 2.2 m, and 1.5 m at La Silla Observatory (Della Valle & Pakull 1991). The spectra showed the presence of emission lines (Hα, Hβ, Hγ, He I λ5876, He II λ4686, and N III λ4640) which are characteristic of X-ray novae, such as V616 Mon, V2107 Oph, Cen X-4, and V404 Cyg.

From 1991 January 17 until 1991 April 22, Nova Muscae 1991 was observed regularly with *IUE*, approximately every 10 days with both the short-wavelength camera (SWP) and long-wavelength camera (LWP) (Gonzalez-Riestra et al. 1991; Shrader & Gonzales-Riestra 1991). The continuum showed a 2200 Å absorption feature due to intervening interstellar dust. UV emission lines were detected at the very beginning, the brightest being C IV λ1550, N V λ1240, O V λ1371. Mg II λ2800 was seen marginally in absorption. In late January a prominent He II λ1640 line appeared in the spectrum, and the O V λ1371 line strengthened.

[1] Based on observations with the NASA/ESA *Hubble Space Telescope* obtained at the Space Telescope Science Institute, which is operated by the Association of Universities for Research in Astronomy, Inc., under NASA contract NAS5-26555.

[2] Space Telescope Science Institute, 3700 San Martin Drive, Baltimore, MD 21218 (postal address for F.H.C.).
[3] Center for Astrophysics, University of Science and Technology of China, Hefei, Anhui 230026, People's Republic of China.
[4] Affiliated with the Astrophysics Division, Space Science Department of ESA.
[5] On leave from University of Catania.
[6] Compton Observatory Science Support Center, Code 6681, NASA/Goddard Space Flight Center, Greenbelt, MD 20771.
[7] On leave from Instituto di Astrofisica Spaziale, CNR, Frascate, Italy.
[8] On leave from Osservatorio Astronomico di Torino, Italy.
[9] Danish Space Research Institute, Gl. lundtoftevej 7, DK-2800 Lyngby, Denmark.

In this paper we present and discuss *Hubble Space Telescope* (*HST*) FOS and FOC observations of Nova Muscae 1991 obtained on 1991 May 14–15. We find a nearly featureless continuum with broad 2200 Å absorption feature and no Balmer jump. We model the FOS spectrum including previous multiepoch *IUE*, optical, and X-ray data using a simple blackbody accretion disk model. In § 2 we present the FOS and FOC observations. A simple model of a steady state accretion disk around a black hole is described in § 3; § 4 gives the spectral fitting results and the analysis of the spectral evolution of Nova Muscae 1991 in light of the above simple model. Finally, the results are discussed in § 5, and the main conclusions are summarized in § 6.

2. OBSERVATIONS

2.1. *Status of HST Observations*

Nova Muscae 1991 was observed several times with *HST*, as summarized in Table 1. The FOC observations on 1991 May 14 and FOS observations on 1991 May 15 were successful, while the GHRS observations on 1991 May 16–17 failed for reasons not yet clarified. A second FOS observation on 1991 October 5 did not detect the nova, possibly because the source was by then too faint for the FOS sensitivity.

2.2. *FOC Observations*

The FOC observations on 1991 May 14 were obtained with medium-width filters F152M, F253M, and F346M, and narrow-band filter F501N (see details in Paresce 1990) with the goal of measuring the UV-optical spectral energy distribution and searching for traces of extended emission from ejecta associated with the outburst. In all four images the nova was detected with optimal exposures. Visual inspection of the images revealed no evidence of extended emission from ejected material. This result places an upper limit of 0.″065 to the nova angular diameter (i.e., the FWHM of the PSF core) in mid-May.

2.3. *FOS Observations*

The FOS spectra were obtained on 1991 May 15 using high-resolution gratings G190H, G270H, and G400H. The spectra cover the region between 1573 and 4823 Å with two wavelength overlaps (2232–2316 Å and 3256–3281 Å). For each grating five exposures of 240 s duration were taken. We averaged the fluxes at the two overlaps (for each grating we have five mean fluxes at each wavelength overlap). We clipped 20 noisy points at the two edges of each spectrum so that the final spectral coverage is 1581–4807 Å.

Figure 1 shows the mean FOS spectrum of Nova Muscae on 1991 May 15 binned to 2 Å pixel^{-1}. To construct the mean spectrum, we averaged the five exposures taken at each grating setting, and multiplied the G190H and G400H spectra by factors of 1.018 and 0.900 to match the G270H spectrum in the wavelength overlap regions. The mismatch could be due to calibration uncertainties or to time variations. Calibration uncertainties are believed to be less than a few percent (G. Hartig 1991, private communication). We found time variations to be generally less than a few percent among the five exposures. The exception is the fifth G190H spectrum, which is 30% low due to a premature exit of the star from the 1″ entrance aperture. An hour elapsed between the exposures with different grating settings, so the 11% difference between G270H and G400H could be due to intrinsic variation of the source. The four diamond symbols in Figure 1 represent the FOC observations using filters F125M, F253M, F346M, and F501N. The FOC fluxes match the FOS spectra fairly well.

2.4. *Reddened Power-Law Continuum*

The most prominent spectral feature is the interstellar 2200 Å absorption. Least-squares fits in terms of reddened power-law models ($f_\nu \propto \nu^\alpha$) to the spectrum yielded best-fit $\alpha = 0.301 \pm 0.024$ and $E(B-V) = 0.287 \pm 0.004$, and $\chi^2_{\rm min} = 3015$ with 1340 degrees of freedom. The quoted uncertainties are 1 σ two-parameter confidence intervals (Lampton, Margon, & Bowyer 1973) derived from a reduced $\chi^2 = 2.25$. In our fits we have used the extinction curve given by Seaton (1979) for $\lambda < 3704$ Å and by Nandy et al. (1975) for $\lambda > 3704$ Å. The power-law slope α is highly correlated with $E(B-V)$, the covariance coefficient between them being +0.95. The model shown in Figure 2 is the best fit. Because the shape of the 2200 Å feature does not fit perfectly, there may be a systematic error in our measured $E(B-V)$ in addition to the quoted uncertainty. We excluded noisy data points and the emission and absorption lines from the spectral fitting. For comparison we plot the best-fitting curves corresponding to $E(B-V) = 0.25$ (see lower dotted curve in the short-

TABLE 1

HST OBSERVATIONS OF NOVA MUSCAE 1991

DATE (1991)	UT (hr)	INSTRUMENT	GRATING OR FILTER	WAVELENGTHS (Å)	RESOLUTION (Å)	RESOLUTION (s)	STATUS
May 14	07.655–08.155	FOC	F152M	1500	188	1800	OK
	09.136–09.636		F253M	2540	236	1800	OK
	10.751–11.251		F346M	3450	432	1800	OK
	12.358–12.858		F510N	5010	74	1800	OK
May 15	12.637–12.987	FOS	G190H	1573–2316	1.5	240	Good spectra
	14.238–14.584		G270H	2232–3281	2.1	240	Good spectra
	15.835–16.185		G400H	3256–4823	3.1	240	Good spectra
May 16	21.326–22.814	GHRS	G160M	1520–1555	0.07	...	No target found
May 17	03.533–05.021			1600–1635	0.07	...	No target found
	08.307–08.890		G270M	2780–2825	0.09	...	No target found
	09.781–10.357			2830–2875	0.09	...	No target found
	12.826–13.146		G140L	1275–1550	0.57	...	No target found
Oct 05.....	13.880–14.467	FOS	G190H	1573–2316	1.5	...	No target found
	15.487–16.154		G270H	2232–3281	2.1	...	No target found
	17.077–17.744		G400H	3256–4823	3.1	...	No target found

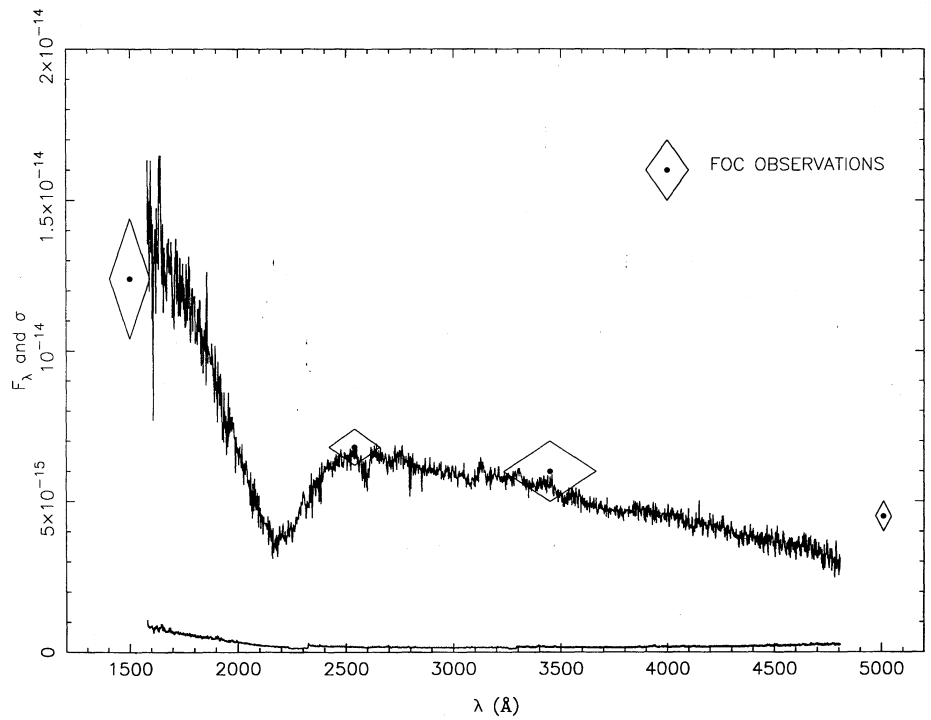

FIG. 1.—Reduced FOS spectrum of Nova Muscae 1991 with wavelength coverage from 1581 to 4807 Å. The 2200 Å absorption feature is clearly shown, but no Balmer jump is seen.

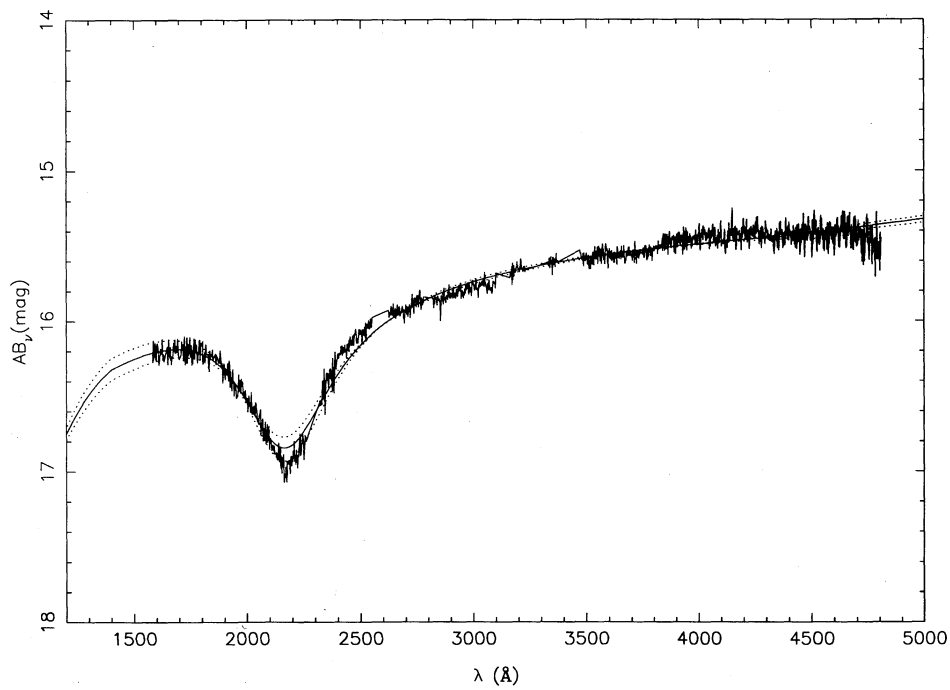

FIG. 2.—Best-fit model with $\alpha = 0.30$ and $E(B-V) = 0.29$ (*solid curve*). We have excluded noisy data points and the emission and absorption lines in the spectral fitting. For comparison we plot the best-fitting curves corresponding to $E(B-V) = 0.25$ (*lower dotted curve in the short-wavelength side*) and 0.33 (*upper dotted curve*).

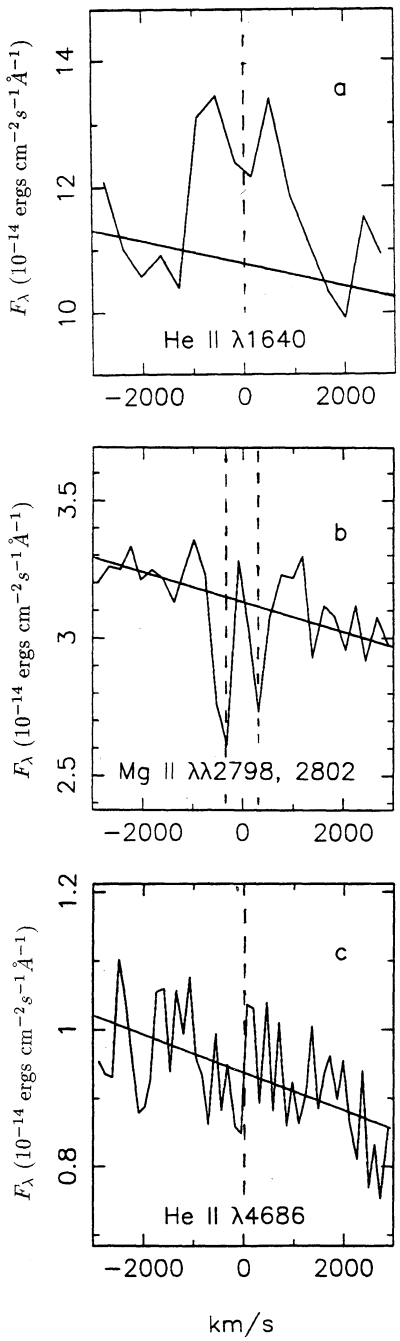

FIG. 3.—Line profiles of He II λ1640 emission line and Mg II λλ2798, 2802 absorption lines are shown in (*a*) and (*b*). The He II λ4686 region is also shown in (*c*), but the He II λ4686 emission line disappears.

wavelength side of Fig. 2) and to $E(B-V) = 0.33$ (see upper dotted curve).

We note that the best-fit power-law spectrum is close to the $f_\nu \propto \nu^{1/3}$ spectrum which is the signature of an extensive optically thick blackbody accretion disk model in steady state with $T \propto R^{-3/4}$ (Pringle 1981).

2.5. *Line Features*

Several line features are visible in the FOS spectrum. Figures 3*a*, and 3*b* show the profiles of the He II λ1640 emission line and the Mg II λλ2798, 2802 absorption lines. For comparison the He II λ4686 region is shown in Figure 3*c*. The He II λ1640 line is in emission with a flux of 2.3×10^{-13} ergs cm^{-2} s^{-1}, and an equivalent width of 2.1 Å. Its velocity profile has a FWHM of 1900 km s^{-1} and may be double-peaked (see Fig. 3). However, no He II λ4686 emission line was found. The interstellar Mg II λλ2798, 2802 absorption features have intensities of 1.7×10^{-14} ergs cm^{-2} s^{-1} and 9.0×10^{-15} ergs cm^{-2} s^{-1}, and equivalent widths of 0.54 and 0.29 Å, respectively. There are some unidentified features, for example, near 2600 Å absorption and 3140 Å emission features.

2.6. *IUE and Optical Observations*

To investigate the spectral evolution of Nova Muscae 1991, we need to consider the *HST* observations in the context of data taken at different wavelengths and at different times. We observed Nova Muscae 1991 with the *International Ultraviolet Explorer* (*IUE*) satellite at 12 epochs between 1991 January 17 and 1991 April 22. In this paper we use the *IUE* spectra only for continuum spectral fitting. We excluded the noise-limited regions $\lambda \geq 2000$ Å for SWP spectra and $\lambda \leq 2400$ Å for LWP spectra. Detailed discussions of the *IUE* observations will be given elsewhere (Shrader 1992).

We also collected observations of Nova Muscae 1991 from the literature (see Table 2). Two spectra covering around 4000–8000 Å are presented by Della Valle et al. (1991a). We first fitted each spectrum with a continuum, then measured the continuum flux at 20 Å intervals. Because their 1991 May 19 spectrum was taken under nonphotometric conditions, only relative fluxes are available. Assuming the source to decline monotonically between 1991 May 15 and May 19, we obtained approximate fluxes by using the wavelength overlap region between our FOS spectrum and their spectrum taking due account of the 4 day time difference and the nominal decay rate of ~ 0.02 mag day^{-1}.

3. BLACKBODY ACCRETION DISK MODELS

The effective temperature distribution for a steady state disk around a black hole without the irradiation effect is (Czerny, Czerny, & Grindlay 1986)

$$T^4 = \frac{3GM\dot{M}}{8\pi\sigma R^3}\left(\frac{1}{1-r'} - 2\frac{\sqrt{r'}}{\sqrt{1-r'}}\right)$$
$$\simeq (2054\ \mathrm{K})^4\left(\frac{m\dot{m}}{r^3}\right)\left(\frac{1}{1-r'} - 2\frac{\sqrt{r'}}{\sqrt{1-r'}}\right), \quad (1)$$

where M is the mass of the central compact object, $\dot{M}$ is the mass transfer rate, R is the radius from the compact object, $m = M/M_\odot$, $\dot{m} = \dot{M}/(10^{-9}\ M_\odot\ \mathrm{yr}^{-1})$, $r = R/10^{11}$ cm, $r_{\rm in} = R_{\rm in}/10^{11}$ cm, $r' = 1.5R_s/R$, and $R_s = 2GM/c^2$ is the Schwarzschild radius. $T_{\rm out}$ and $T_{\rm max}$ are temperatures at the outermost and innermost disk. Thus $T_{\rm out} \propto (M\dot{M})^{1/4}R_{\rm out}^{-3/4}$, where $R_{\rm out}$ is the outermost radius of the disk. If we let the innermost radius be $R_{\rm in} = \zeta R_s$, where we take $\zeta = 3$ for a Schwarzschild black hole, then the maximum value of the temperature in the disk is given by (Czerny et al. 1986)

$$T_{\rm max} = 0.369\left(\frac{\dot{M}_9}{M_{1.4}^2}\right)^{1/4}(\mathrm{keV}) \simeq (5.07 \times 10^6\ \mathrm{K})\left(\frac{\dot{m}}{m^2}\right)^{1/4}, \quad (2)$$

where $\dot{M}_9 = \dot{m}$ and $M_{1.4} = m/1.4$. $T_{\rm max}$ is reached at a radius $R = 4.8R_s$.

TABLE 2

COLLECTED OBSERVATIONS OF NOVA MUSCAE 1991 AT DIFFERENT WAVELENGTH BANDS AND DIFFERENT OBSERVING DATES

Symbol Used in Figures 4 and 5	Observing Date (1991)	Wavelength Band	Dereddened AB_ν (mag)[a]	References
Circle	Jan 15	4200–8000 Å	See Fig. 4	1
Triangle	Jan 17	1300 Å	11.50	2
		1500 Å	11.80	
		3100 Å	12.15	
		5500 Å	12.26	
Filled square	Jan 20–21	3.5–100 keV	See Fig. 4	3
Asterisk	Apr 19–25	5500 Å	13.94	4
Small circle	May 19	4000–7200 Å	See Fig. 4	1
Star	May 31	10 keV	20.10	5
		100 keV	22.90	
Plus sign	Jun 7	5500 Å	14.94	6
Open cross	Jun 8	5500 Å	15.04	6

[a] $AB_\nu = -2.5 \log f_\nu - 48.6$, where f_ν is in units of ergs cm^{-2} s^{-1} Hz^{-1}.

REFERENCES.—1: Della Valle et al. 1991a; 2: Gonzalez-Riestra et al. 1991; 3: Sunyaev et al. 1991b; 4: Bailyn 1991a; 5: Sunyaev et al. 1991a; 6: Bailyn 1991b.

The observed flux from the source, assuming blackbody radiation from each radius in the disk and no Galactic absorption, is

$$f_\nu = f_0 \frac{\cos i}{d^2} (m\dot{m})^{2/3} \nu_{15}^{1/3} \int_{x_{\rm in}(\nu)}^{x_{\rm out}(\nu)} \frac{x^{5/3} dx}{e^x - 1}, \quad (3)$$

where $d = D/\text{kpc}$, $\nu_{15} = \nu/10^{15}$ Hz, D is the source distance, i is the disk inclination angle, $x_{\rm out}(\nu) = h\nu/(kT_{\rm out})$, $x_{\rm in}(\nu) = h\nu/(kT_{\rm max})$, and

$$f_0 = \left(\frac{16\pi}{3}\right)\left(\frac{3G}{8\pi\sigma}\right)^{2/3}\left(\frac{h}{c^2}\right)\left(\frac{k}{h}\right)^{8/3}\left(\frac{M_\odot^2}{10^9 \text{ yr}}\right)^{2/3}\frac{10^5}{(\text{kpc})^2}$$
$$\simeq 2.9 \times 10^{-26} \text{ ergs cm}^{-2} \text{ s}^{-1} \text{ Hz}^{-1}. \quad (4)$$

G, σ, h, c, and k in equations (1), (3), and (4) are the standard physical constants.

A glance at Figure 4 shows that the blackbody disk spectrum has two (*low* and *high*) "shoulders" straddling the $\nu^{1/3}$ power law at frequencies ν_L and ν_H. Here ν_H corresponds to $h\nu_H = kT_{\rm max}$ in the inner disk. For $\nu \ll \nu_L$, the Rayleigh-Jeans tails of the coolest disk elements dominate, and we have

$$f_\nu = (8.3 \times 10^{-26} \text{ ergs cm}^{-2} \text{ s}^{-1} \text{ Hz}^{-1}) \times \frac{\cos i}{d^2} (m\dot{m})^{1/4} \nu_{15}^2 r_{\rm out}^{5/4}, \quad (5)$$

where $r_{\rm out} = R_{\rm out}/10^{11}$ cm. For $\nu_L \ll \nu \ll \nu_H$, the disk spectrum approaches a $\nu^{1/3}$ power law

$$f_\nu = f_0 \frac{\cos i}{d^2} (m\dot{m})^{2/3} \nu_{15}^{1/3} \int_0^\infty \frac{x^{5/3} dx}{e^x - 1}, \quad (6)$$

where the integral evaluates to 1.9.

The frequencies ν_L and ν_H represent the positions of the *low* and *high* "shoulders" in the disk spectrum. Equating equations (5) and (6), we find ν_L, the frequency at which the $\nu^{1/3}$ power-law spectrum turns over into a ν^2 power law:

$$\nu_L \simeq (4.2 \times 10^{14} \text{ Hz}) \left(\frac{T_{\rm out}}{10^4 \text{ K}}\right) \propto \left(\frac{M\dot{M}}{R_{\rm out}^3}\right)^{1/4}. \quad (7)$$

The frequency ν_H at which the $\nu^{1/3}$ power-law spectrum starts to turn over into a Wien spectrum, exponentially decreasing with increasing frequency, is

$$\nu_H = \frac{kT_{\rm max}}{h} \simeq (2.083 \times 10^{16} \text{ Hz}) \left(\frac{T_{\rm max}}{10^6 \text{ K}}\right) \propto \left(\frac{\dot{M}}{M^2}\right)^{1/4}. \quad (8)$$

From the above equations we note that the disk spectrum has the following characteristics:

1. The flux f_ν is proportional to d^{-2} and $\cos i$;
2. When M increases, f_ν increases, ν_L moves toward higher frequencies, but ν_H moves toward lower frequencies;
3. When $\dot{M}$ increases, f_ν increases, and both ν_L and ν_H increase;
4. When $R_{\rm out}$ increases, f_ν increases too, but ν_L decreases.

For X-ray binary systems, the central compact object may be a neutron star, or possibly a black hole. We should, therefore, consider the relativistic effects on the observed spectrum. In this paper we only consider the local blackbody emission for a disk around a central nonrotating compact object. In other cases the spectrum produced by the accretion disk may not show a $\nu^{1/3}$ power law (Laor & Netzer 1989). We adopt Cunningham's (1975) transfer function which describes the relativistic corrections on the disk radiation for the case of a Schwarzschild black hole. We also adopt the simplified formulas by Czerny et al. (1986) in our calculations. The relativistic corrections for a Schwarzschild black hole affect mainly the high-frequency tail. In the case of $i \sim 90°$, the flux is still relatively strong because of the gravitational focusing effect, but no $\nu^{1/3}$ power-law spectrum is seen.

4. THE SPECTRAL EVOLUTION

4.1. *Observational Constraints*

Figure 4 compares observations with a series of model disk spectra. The parameters of the disk models are given in the figure. The observed spectra and photometric data points were dereddened by an extinction of $E(B-V) = 0.29$. Note that the monochromatic magnitude AB_ν is defined as $-2.5 \log f_\nu - 48.6$. Figure 5 enlarges the region of Figure 4 in which we are most interested. The longest spectrum is the *HST*/FOS

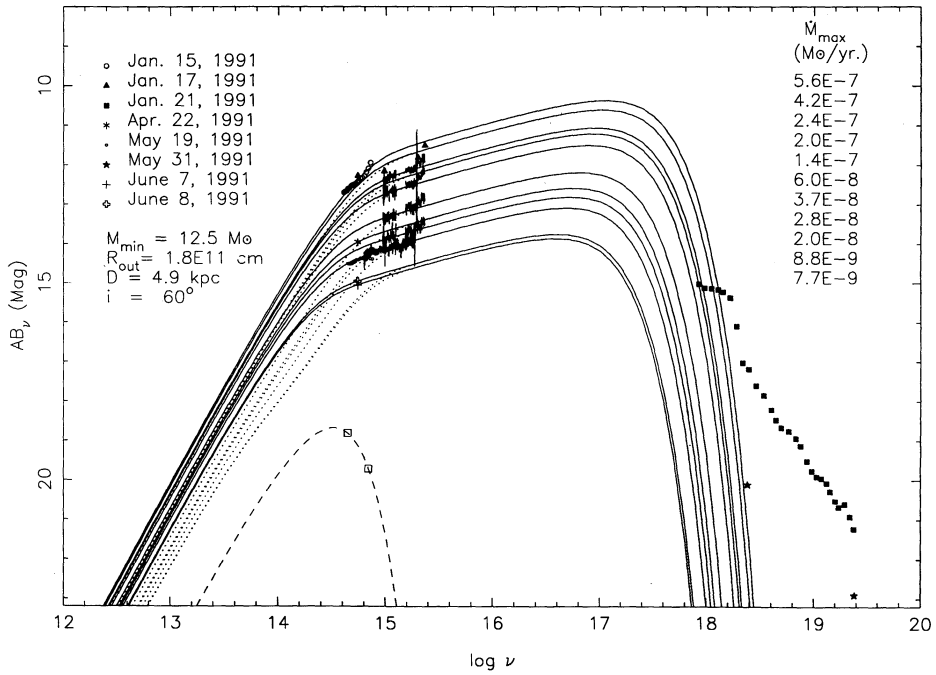

FIG. 4.—Observed spectra in optical, UV and X-ray bands and the spectral fitting. The observing times corresponding to the symbols used are shown in the upper left corner. The parameters i, D, and the estimated M_{min}, R_{out}, and a set of $\dot{M}_{max}$ are also shown (*see solid curves*). The longest spectrum is the *HST*/FOS observations. Only four *IUE* spectra (SWP+LWP) were shown in the figure, and they were observed from the top to the bottom on 1991 January 17, Feburary 6, March 15, and April 22, respectively. The dereddened AB_ν magnitudes of the prenova of Nova Muscae 1991 at 4350 and 5500 Å (*open squares*), and the best-fitting spectrum of a blackbody with temperature of 5550 K (*dashed curve*) are also plotted in the figure. From this we obtain the source distance $D \simeq 8.0$ kpc. The dotted curves in the figure are the predictions by the disk instability models with a cooling front.

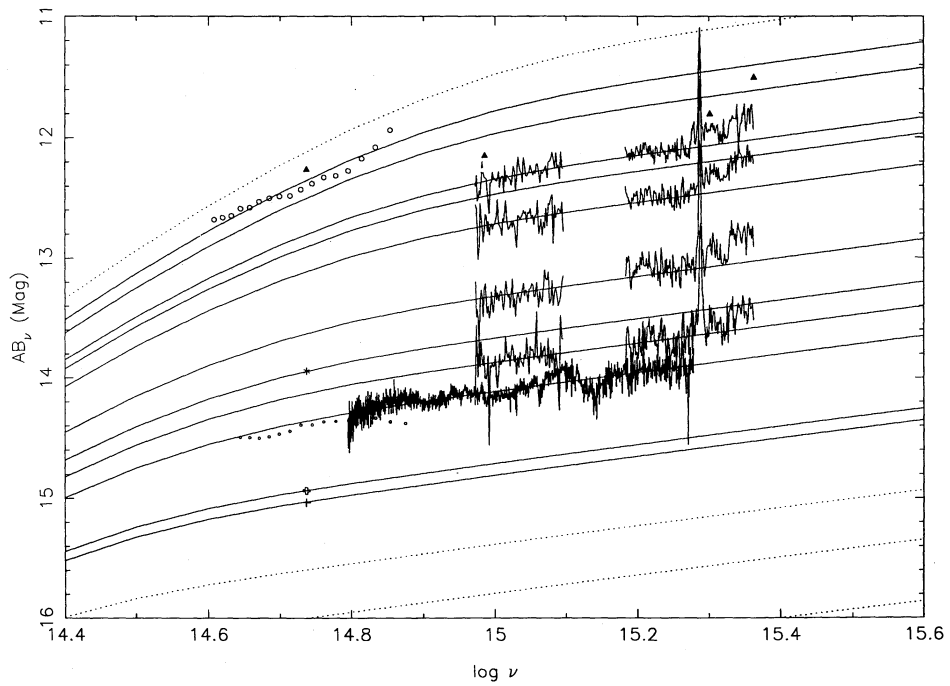

FIG. 5.—Enlarged region of Fig. 4 to see the spectral fitting in detail

observation. We selected four *IUE* spectra in Figures 4 and 5 to prevent crowding. The epochs of the *IUE* spectra are 1991 January 17, February 6, March 15, and April 22 from the top to the bottom. We also plot two data points from *B*- and *R*-magnitudes of the prenova from Della Valle et al. (1991a) and a best-fit blackbody spectrum of 5550 K in Figure 4 (see details in § 5). The dotted curves in Figure 4 are the predictions by the disk instability models with a cooling front (also see details in § 5).

In Figure 4 we note several features of the observed spectra:

1. At a very early stage of the outburst, the optical continuum on 1991 January 15 (circle symbol in the figure) was much steeper than a $\nu^{1/3}$ behavior but flatter than a ν^2 power law. This means that ν_L was located near the optical wavelengths 4000–8000 Å, thus $T_{\rm out} \sim 1.2 \times 10^4$ K, which provides an interesting constraint for our spectral fitting.

2. The X-ray data obtained on 1991 January 20–21, and 1991 May 31 (filled square and star symbols) follow a power law with photon index 2.2–2.3, much flatter than the exponential cutoff at high frequency in the disk models. This indicates that the X-ray flux must consist not only of a blackbody accretion disk component, but must include other radiation mechanisms, for example, Comptonization from a hot disk corona (Czerny & Elvis 1987; Mineshige et al. 1990). Therefore, we have constrained our disk models to keep the predicted X-ray flux below the observed X-ray flux.

3. The fluxes in the UV, optical, and lower energy X-ray bands decreased in an orderly way with the time. In fitting the lower energy X-ray data of 1991 January 20–21, we require the theoretical curve that predicts the X-ray flux to obey the observed time sequence.

4.2. *Fitting Procedure*

The theoretical disk spectrum depends on several parameters: i, D, M, $\dot{M}$, and $R_{\rm out}$. For a given i (say, 60°) and a given D (say, 4.9 kpc), we can use the three constraints above to estimate the lower limit mass $M_{\rm min}$, the disk radius $R_{\rm out}$, and the set of $\dot{M}$ values corresponding to the observations at different times. The procedure consists of the following steps:

Step 1—Determine $(M\dot{M})$ on 1991 January 21. For the given values of i and D, we select M (say, 1 $M_\odot$), and $R_{\rm out}$ (say, 10^{11} cm), and then adjust $\dot{M}$ until the theoretical spectrum obeys the time sequence, that is its $\nu^{1/3}$ power law is (4 days × 0.02 mag/day ~) 0.1 mag lower than the first *IUE* spectrum of 1991 January 17. Thus we find the UV-optical flux, and $(M\dot{M}) = C_1$ (see eq. [6]) on 1991 January 21.

Step 2—Determine $M_{\rm min}$. From the set of calculated theoretical spectra we can also find another spectrum which passes through the observed low-frequency data point (filled square symbol) of the X-ray observations on 1991 January 20–21. This point determines the ν_H position corresponding to a constant value of $(\dot{M}/M^2)$, say C_2 (see eq. [8]). Therefore, $M = (C_1/C_2)^{1/3}$ is obtained. Using this value of M with a set of selected $\dot{M}$ we can get one theoretical spectrum which not only passes through the low-energy data point of the X-ray observations on 1991 January 20–21, but also obeys the time sequence at optical-UV band. Note that the mass M determined in this way is unique for the given i and D and represents the lower limit $M_{\rm min}$. For M smaller than $M_{\rm min}$, a larger $\dot{M}$ is needed to match the UV-optical flux, therefore, a higher $\nu_{\rm H}$ appears to predict a higher model X-ray flux than that of the observed low-energy data point, which is the second constraint mentioned in § 4.1. On the other hand, if we take a M larger than $M_{\rm min}$, the model predicts an X-ray flux lower than the observations, which is consistent with the constraints. We use only the low-energy point of the X-ray observations on 1991 January 20–21 to determine $M_{\rm min}$, because any other data point used would cause the model to predict a higher flux than the observed flux of the low-energy point. We also did not use the X-ray observations on 1991 May 31 for the same reason.

Step 3—Determine $R_{\rm out}$. Repeating Step 1 to determine $(M\dot{M})$ on 1991 January 15, we then find $R_{\rm out}$ by matching the optical slope of 1991 January 15, because of $\nu_L \propto (M\dot{M}/R_{\rm out}^3)^{1/4}$ (see eq. [7]).

Step 4—determine $\dot{M}_{\rm max}$. Let $\xi = M/M_{\rm min}$; we have $M = \xi M_{\rm min}$. From the derived values of $M_{\rm min} = M/\xi$ and $R_{\rm out}$, we can find theoretical curves that pass through the observed spectra and the observed data points in Figure 4 (solid curves). The corresponding mass transfer rates are the maximum values $\dot{M}_{\rm max} = \xi\dot{M}$, which are listed in Table 3.

4.3. *Fitting Results*

Table 3 lists our spectral fitting results. We selected $D = 10.5$, 4.9, 1.8 kpc, $i = 60°$ as models A, B, and C, and selected $i = 0°$, 85°, $D = 4.9$ kpc as models D and E. The Eddington mass transfer rate is $\dot{M}_{\rm Edd} = 3.88 \times 10^{-8}\ M\ {\rm yr}^{-1}$. (Laor & Netzer 1989) where M is in units of $M_\odot$. Using $M_{\rm min}$ instead of M, we have the quantity $\dot{M}'_{\rm Edd} = \dot{M}_{\rm Edd}/\xi = 3.88 \times 10^{-8}\ M_{\rm min}\ {\rm yr}^{-1}$, which is also listed in Table 3 for comparison. Note that the values of $M_{\rm min}$ for all five models are larger than 4 $M_\odot$.

The model parameters cannot yet be uniquely determined until the distance to the system or the binary period can be estimated. But they imply interesting constraints, including lower limits on the mass of the central compact object as a function of the assumed distance to the system.

4.4. *Spectral Evolution*

From Table 3 we can see the estimated $\dot{M}_{\rm max}$ changing with the time. To determine a characteristic decay time τ, we plot $\log(M\dot{M})$ against the observing date in Figure 6 for models A, B, and C. If $\dot{M}$ decays exponentially, then we expect

$$(\dot{M}M) = (\dot{M}_{\rm Edd}\,M)\eta e^{-(t-t_0)/\tau} = (\dot{M}'_{\rm Edd}\,M_{\rm min})\eta e^{-(t-t_0')/\tau}, \quad (9)$$

where η is a coefficient, $t_0' = t_0 + 2\tau \ln \xi$. If $\dot{M} \leq 0.3\dot{M}_{\rm Edd}$, then the thin disk assumption stands (Laor & Netzer 1989). From the best fit in Figure 6 we find that the decay time is $\tau \sim 43$ days for all of the models. We also find values of t_0' which are 77, 47, and 9 days for the models A, B, and C when $\eta = 0.3$. This indicates that in model C the thin disk assumption is valid over the course of the decay, because the outburst started at $t = 15$ days. In models A (if $\xi < 2.1$) and B (if $\xi < 1.5$), however, the thin disk condition breaks down in the early decline.

4.5. *The Binary Period*

For a main-sequence companion in the binary system, the mass (Warner 1976) is

$$M_c \sim \frac{P}{8.3\ {\rm hr}}\,M_\odot, \quad (10)$$

where P is the orbital period in hours. So the mass ratio is

$$q = \frac{M}{M_c} \sim \frac{8.3M}{P}. \quad (11)$$

TABLE 3

SPECTRAL FITTING RESULTS

Model	A	B	C	D	E
i (°)	60	60	60	0	85
d (kpc)	10.5	4.9	1.8	4.9	4.9
M_{min} ($M_\odot$)	27	12.5	4.1	7.0	37
R_{out} (10^{11} cm)	3.6	1.8	0.7	1.2	4.5
P_{max} (hr)	18.5	9.8	4.4	7.5	21.6

	$\dot{M}_{max}(=\xi\dot{M})(M_\odot\ yr^{-1})$				
DATE (UT)	A	B	C	D	E
15	2.8E−6	5.6E−7	7.2E−8	3.8E−7	2.4E−6
17	1.9E−6	4.2E−7	5.7E−8	2.6E−7	1.9E−6
17	1.1E−6	2.4E−7	3.1E−8	1.5E−7	1.1E−6
20	9.7E−7	2.0E−7	2.6E−8	1.3E−7	9.0E−7
20	1.0E−6	2.2E−7	2.5E−8	1.4E−7	9.2E−7
23	1.1E−6	2.3E−7	2.7E−8	1.4E−7	9.5E−7
37	6.6E−7	1.4E−7	1.9E−8	9.3E−8	6.1E−7
49	3.4E−7	1.1E−7	1.3E−8	7.2E−8	4.9E−7
59	2.3E−7	7.3E−8	8.7E−9	4.6E−8	3.1E−7
74	2.6E−7	6.0E−8	7.8E−9	3.6E−8	2.8E−7
86	3.1E−7	6.5E−8	8.5E−9	4.1E−8	2.9E−7
109	1.7E−7	3.7E−8	5.0E−9	2.4E−8	1.7E−7
112	1.4E−7	2.8E−8	3.8E−9	1.8E−8	1.3E−7
135	9.1E−8	1.4E−8	2.8E−9	1.3E−8	8.9E−8
158	3.5E−8	7.7E−9	1.1E−9	4.9E−9	3.6E−8
159	4.0E−8	8.8E−9	1.2E−9	5.5E−9	4.1E−8
$\dot{M}'_{Edd}(=\dot{M}_{Edd}/\xi)$... ($M_\odot\ yr^{-1}$)	1.1E−6	4.9E−7	1.6E−7	2.7E−7	1.4E−6

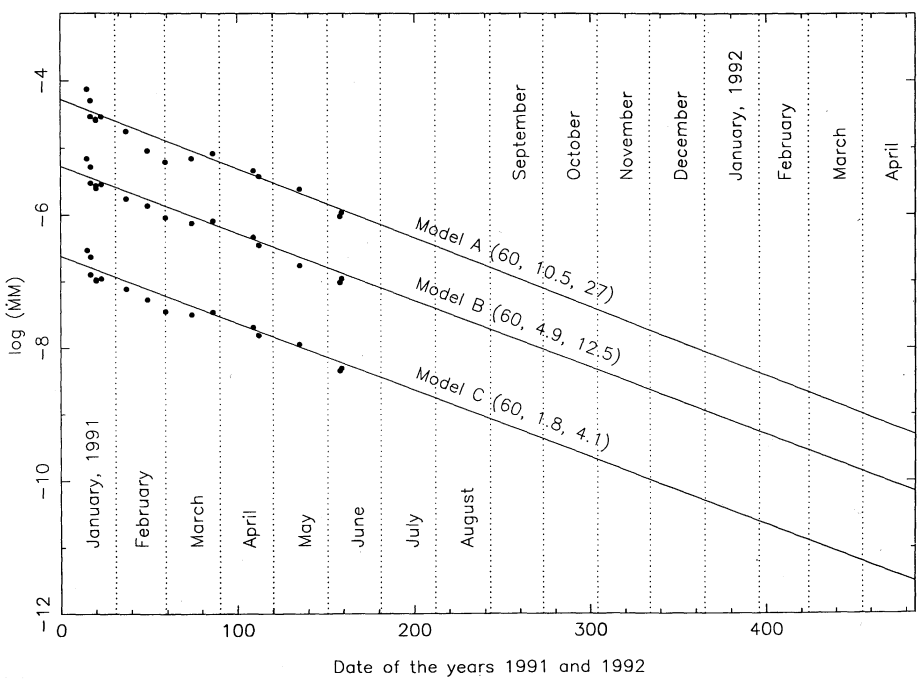

FIG. 6.—($\dot{M}M$) decays with time for the models A, B, and C. The numbers following each model are the inclination angle (in units of *degree*), distance (in units of *kpc*), and the lower limit mass (in units of $M_\odot$ estimated from the spectral fitting). The straight lines are the best fit to the data points in the figure; the slopes of the lines determine the decay time $\tau \sim 43$ days.

If the accretion disk fills 80% of the radius R_L of the Roche lobe, where (eq. [2] of Eggleton 1983)

$$\frac{R_L}{a} = f(q) = \frac{0.49q^{2/3}}{0.6q^{2/3} + \ln(1 + q^{1/3})}, \quad (12)$$

and a is the separation between the primary and the companion, which is given by Kepler's law, then we have

$$R_{\rm out} = 0.8R_L = 0.8f(q)a = 0.8f(q)\left(\frac{G}{4\pi^2}\right)^{1/3} \times [(3600P)^2(2 \times 10^{33}M)(1 + 1/q)]^{1/3}. \quad (13)$$

We note that q in equation (13) is also a function of the period P (see eq. [11]). From the estimated values of $R_{\rm out}$, and using $M_{\rm min}$ instead of M, we obtain the maximum period $P_{\rm max}$ by solving equation (13). The values of $P_{\rm max}$ for our five selected models are also listed in Table 3.

5. DISCUSSION

The predicted maximum orbital periods $P_{\rm max}$ are model dependent, ranging from $\sim$4.4 to $\sim$21.6 hr, in our selected models. Recent observations of Nova Muscae 1991 by Bailyn (1991b) suggest that the period is $P \sim 10.5$ hr. In this case $M_{\rm min}$ is 13.4 $M_\odot$ in the case of $D = 5.1$ kpc, $i = 60°$ and $R_{\rm out} = 1.9 \times 10^{11}$ cm.

Figure 7 shows the determined $M_{\rm min}$ as a function of assumed source distance D and disk inclination angle i. The numbers near the symbols in the figure represent the orbital periods obtained from the best fit to the observations. The three shaded symbols represent the systems with period 10.5 hr for three different disk inclination angles. The most probable $M_{\rm min}$ is between 10 and 15 $M_\odot$, depending on what the inclination angle i is (dotted lines). The corresponding source distance is between 2 and 7 kpc. The more recent period observations by Schmidtke & Cowley (1992) show $P \sim 8.5$ hr (filled symbols in Fig. 7). This period gives the most probable $M_{\rm min}$ between 8.0 and 12.3 $M_\odot$ (dashed lines), and the corresponding source distance between 1.6 and 5.5 kpc. Note that since we used $M_{\rm min}$ as the mass of the central object in determining the period, the real periods must be shorter than those marked in the figure, because the larger the mass, the shorter the period. In this case the symbols should move up and the corresponding periods decrease. The dashed lines connecting filled symbols will go up and right in the figure.

We have also assumed the disk filling 80% of the Roche lobe and $R_{\rm in} = 3R_s$ (Schwarzschild black hole) in determining the period. If the percentage is 60%, we still have $M_{\rm min} > 5\ M_\odot$. But if we take $R_{\rm in} = 100R_s$ (e.g., for a magnetized neutron star, $R_{\rm in} = R_M$, at which the magnetic pressure is equal to the ram pressure, is much larger than $3R_s$), the estimated $M_{\rm min}$ is only slightly larger than $\sim 1\ M_\odot$ (Frank, King, & Raine 1985). Therefore, Nova Muscae 1991 is a strong black hole candidate if the disk fills 60% of the Roche lobe and if the inner radius of disk is small enough, say, $3R_s$.[10]

If Bailyn's $\sim$10.5 hr period is correct, then the Roche lobe can be filled by a main-sequence companion star, with a mass $M_c \simeq 1.3\ M_\odot$ (see eq. [10]). We then estimate the radius of the companion $R_c \simeq 1.2\ R_\odot$ by using of equation (11) of Patterson (1984). Della Valle et al. (1991a) give the magnitudes of the prenova of Nova Muscae 1991 as $m_B \sim 20.9$, $m_R \sim 19.4$. Using a best-fit blackbody of 5550 K with a reddening of

[10] After our paper was accepted, a report by McClintock, Bailyn, & Remillard (1992) gave Nova Muscae's mass function as $3.1 \pm 0.5\ M_\odot$, which provided dynamical evidence that the primary is a black hole. This result is consistent with our analysis.

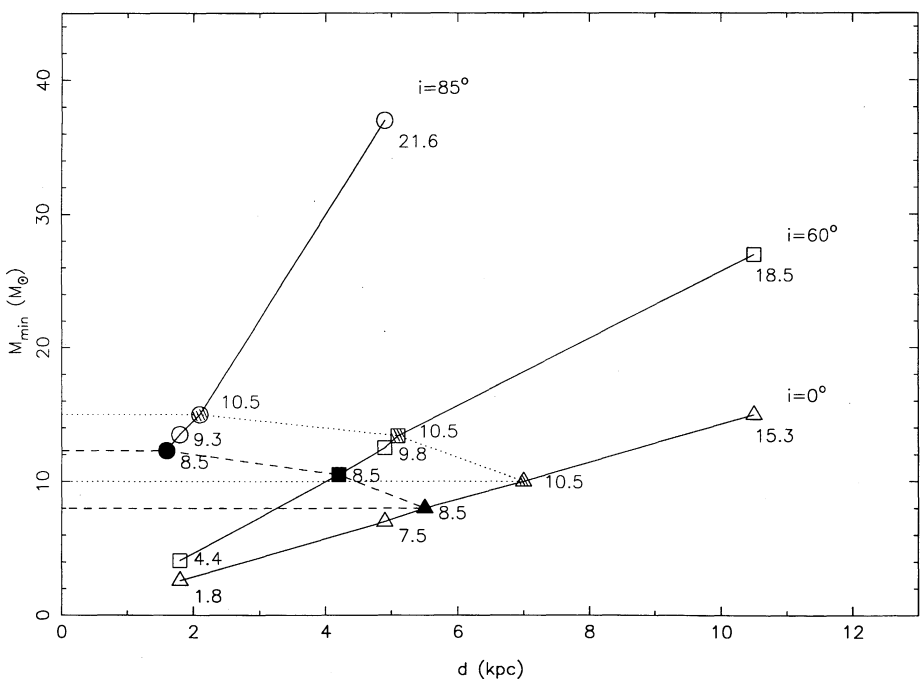

FIG. 7.—Determined $M_{\rm min}$ as a function of assumed source distance d and disk inclination angle i. The numbers near the symbols in the figure represent the orbital periods obtained from the best fit to the observations. Three shaded symbols represent the systems with period 10.5 hr at three different disk inclination angles. Three filled symbols correspond to $P = 8.5$ hr.

$E(B-V) = 0.29$, we obtain $R_c/D \simeq 0.15\ R_\odot$/kpc. We plot the spectrum of a blackbody with temperature of 5550 K in Figure 4 (dashed curve) together with the dereddened prenova AB_v magnitudes at 4350 and 5500 Å (open square symbols). From such a plot we derive the source distance $D \simeq 8.0$ kpc. If Schmidtke & Cowley's 8.5 hr period is true, then the source distance $D \simeq 5.3$ kpc.

In the five selected models we hold the outer disk radius fixed, thus the outer temperature T_{out} declines from $\sim$12,000 K at outburst to $\sim$5000 K in mid-May when the FOS spectra were obtained. According to the disk instability model of Mineshige et al. (1990), there should have been a rapid cooling from 10^4 to $\sim 1.6 \times 10^3$ K as hydrogen recombined in the outer disk. This would have resulted in a fixed outer disk temperature but decreasing radius, causing ν_L to remain near 10^{15} Hz throughout the decline (see dotted curves in Fig. 4). But our FOS spectrum and the optical observations of Della Valle et al. (1991a) do not seem to agree with this disk instability model. The cooling front in the outer disk of Nova Muscae 1991 does not seem to exist. Because the blackbody radiation with temperature $\sim$1600 K peaks at $\sim 10^{14}$ Hz and dominates the spectra during the late decline, it would be enormously helpful to get infrared observations in decline to pin down the evolution of the outer disk temperature.

Despite its simplicity, the blackbody accretion disk model predicts no Balmer jump, which is consistent with the observations, whereas Kurucz model atmospheres always predict a Balmer jump in absorption that is not seen in the data. As an example, the Balmer jump for disk model B using Kurucz model atmospheres is $BJ \geq 0.3$ ($BJ = \log [I_+(3646)/I_-(3646)]$, where $I_+(3646)$ and $I_-(3646)$ are the continuum fluxes at long- and short-wavelength side of the Balmer limit, respectively). The blackbody accretion disk model is obviously a better representation of Nova Muscae 1991 than disk models constructed from Kurucz spectra.

The *IUE* observations show UV excesses in the SWP spectra which are steeper than the $\nu^{1/3}$ power law. The X-ray observations show flatter spectra than the high-frequency tail of the blackbody accretion disk spectrum (Sunyaev et al. 1991b). The X-ray flux also did not decrease exponentially (Sunyaev et al. 1991c). Therefore, to explain the whole spectral evolution of Nova Muscae 1991, other radiation mechanisms are certainly needed to produce sufficient X-ray and EUV fluxes. Further work on this issue is necessary.

6. CONCLUSIONS

The main conclusions of this paper are as follows:

1. The color excess $E(B-V)$ is $\sim$0.29, which is in good agreement with the result obtained by Della Valle et al. (1991b) and by Shrader & Gonzalez-Riestra (1991).
2. The power-law slope $\alpha \sim 0.30$ found from the best fit to the FOS spectrum supports a local blackbody model of an accretion disk around a black hole.
3. The estimated lower limits on the mass of the central compact object, obtained using the observed 8.5 hr period and assuming a disk filling 80% of the Roche lobe and $R_{in} = 3R_s$, are higher than 8.0 $M_\odot$ (or 10 $M_\odot$, if $P = 10.5$ hr), consistent with a black hole primary.
4. The estimated decay time τ of mass transfer rate based on the *HST*, UV, and optical observations is about 43 days, nominally consistent with the observable *e*-folding time of the UV–X-ray light curves.
5. The most likely value of the source distance is $\sim$8 kpc if the period estimate of 10.5 hr is true (or $\sim$6.3 kpc, if $P = 8.5$ hr).
6. We do not see the cooling front predicted by the disk instability model in Nova Muscae 1991.

We wish to thank an anonymous referee for useful comments, J. E. Pringle and Craig Wheeler for useful discussions, Charles Bailyn for sharing data prior to publication, and S. Beaulieu for assistance in FOS data processing. We also thank M. Della Valle for sending us the ESO published spectra of Nova Muscae 1991. Support for this work was provided by NASA through grant number GO 3232.01-91A from the Space Telescopic Science Institute, which is operated by the Association of Universities for Research in Astronomy, Inc., under NASA contract NAS5-26555.

REFERENCES

Bailyn, C. 1991a, IAU Circ., 5259
———. 1991b, preprint
Casares, J., Charles, P. A., & Naylor, T. 1992, Nature, 355, 614
Cunningham, C. T. 1975, ApJ, 202, 788
Czerny, B., Czerny, M., & Grindlay, J. E. 1986, ApJ, 311, 241
Czerny, B., & Elvis, M. 1987, ApJ, 321, 305
Della Valle, M., & Jarvis, B. J. 1991, IAU Circ., 5165
Della Valle, M., Jarvis, B. J., & West, R. M. 1991a, A&A, 247, L33
———. 1991b, Nature, 353, 50
Della Valle, M., & Pakull, M. 1991, IAU Circ., 5167
Eggleton, P. 1983, ApJ, 268, 368
Frank, J., King, A. R., & Raine, D. J. 1985, Accretion Power in Astrophysics (Cambridge: Cambridge Univ. Press)
Gonzales-Riestra, R., Cassatella, A., Wamsteker, W., Shrader, C., Shore, S., & Lund, N. 1991, IAU Circ., 5174
Haswell, C. A., & Shafter, A. W. 1990, ApJ, 359, L47
Lampton, M., Margon, B., & Bowyer, S. 1976, ApJ, 208, 177
Laor, A., & Netzer, H. 1989, MNRAS, 238, 897
Lund, N., & Brandt, S. 1991, IAU Circ., 5161
Makino, F. 1991, IAU Circ., 5161
McClintock, J. E., Bailyn, C., & Remillard, R. A. 1992, IAU Circ., 5499
McClintock, J. E., & Remillard, R. A. 1986, ApJ, 308, 110
Mineshige, S., Kim, S. W., & Wheeler, J. C. 1990, ApJ, 358, L5
Mineshige, S., & Wheeler, J. C. 1989, ApJ, 343, 241
Nandy, K., Thompson, G. I., Jamar, C., Monfils, A., & Wilson, R. 1975, A&A, 44, 195
Osaki, Y. 1974, PASJ, 26, 429
Paresce, F. 1990, The Faint Object Camera Instrument Handbook, Version, 2.0 (Baltimore: STScT)
Patterson, J. 1984, ApJS, 54, 443
Pringle, J. E. 1981, ARA&A, 19, 137
Schmidtke, P. C., & Cowley, A. P. 1992, IAU Circ., 5451
Seaton, M. J. 1979, MNRAS, 187, 73P
Shrader, C. R. 1992, in preparation
Shrader, C. R., & Gonzalez-Riestra, R. 1991, in The Workshop on Nova Muscae 1991, ed. S. Brandt (Lyngby: Danish Space Research Inst.), 85
Sunyaev, R., Jourdian, E., & Laurent, P. 1991a, IAU Circ., 5176
———. 1991b, in The Workshop on Nova Muscae 1991, ed. S. Brandt (Lyngby: Danish Space Research Inst.), 51
———. 1991c, IAU Circ., 5310
Warner, B. 1976, in IAU Symp. 73, The Structure and Evolution of Close Binaries, ed. P. Eggleton, S. Mitton, & J. Whelan (Dordrecht: Reidel), 85